Nuclear Engineering and Technology 53 (2021) 3711–3716

Contents lists available at ScienceDirect

Nuclear Engineering and Technology

journal homepage: www.elsevier.com/locate/net

Original Article

Entropy, enthalpy, and gibbs free energy variations of ^{133}Cs via CO_2-activated carbon filter and ferric ferrocyanide hybrid composites

Joon Hyuk Lee, Dong Hack Suh*

Department of Chemical Engineering, Hanyang University, Wangsimni-ro, Seongdong-gu, Seoul, 133-791, South Korea

ARTICLE INFO

Article history:
Received 18 May 2021
Received in revised form
5 June 2021
Accepted 7 June 2021
Available online 12 June 2021

Keywords:
^{133}Cs
Radionuclide
Activated carbon filter
Ferric ferrocyanide
Thermodynamics
Energy variation

ABSTRACT

The addition of ferric ferrocyanide (Prussian blue; PB) to adsorbents could enhance the adsorption performance of ^{133}Cs. Toward this goal, we present a heterogeneously integrated carbonaceous material platform consisting of PB in direct contact with CO_2-activated carbon filters (PB-CACF). The resulted sample retains 24.39% more PB than vice versa probed by the ultraviolet–visible spectrometer. We leverage this effect to capture ^{133}Cs in the aqueous environment via the increase in ionic strength and micropores. We note that the amount of PB was likely to be the key factor for ^{133}Cs adsorption compared with specific surface characteristics. The revealed adsorption capacity of PB-CACF was 21.69% higher than the bare support. The adsorption characteristics were feasible and spontaneous. Positive values of ΔH^o and ΔS^o show the endothermic nature and increased randomness. Based on the concept of capturing hazardous materials via hazardous materials, our work will be of interest within the relevant academia for collecting radionuclides in a sufficient manner.

1. Introduction

Nuclear energy is touted as a high-volume energy source with minimal land use. Nuclear energy comes with various benefits and drawbacks, which makes it such a controversial energy source [1–4]. Major advantages of nuclear energy include low-cost and high efficiency. On the other hand, there are also disadvantages including the risk of nuclear accidents and radioactive wastes. A meltdown at a nuclear power plant remains a challenge, which is acknowledged from the unfortunate events of Fukushima and Chernobyl [5]. Amongst the radioactive materials, ^{137}Cs is one of the representative radioisotopes [6–8]. Compared to other radionuclides, ^{137}Cs has a large diffusion coefficient once dissolved in water since it has a small hydration radius. While being the most efficient energy source is a big plus of nuclear energy, radioactive waste management makes it more competitive against alternative energy sources. The current technologies can easily capture radionuclides with relative ease, but an efficient system is yet not in place. While corresponding methods have been proposed, they are expensive and/or rely on highly educated control. One potential route to overcome such requirements is physisorption-based adsorption via van der Waals force [9]. The use of adsorption has been intensified, since it can be operated at near-ambient conditions and integrated into current engineering setups [10–13]. Several porous adsorbents including activated carbons, zeolites, and activated carbon filters (ACFs) have been incentivized, but were found to have insufficient ^{137}Cs adsorption capacity without additional surface modification. Ferric ferrocyanide (Prussian blue; PB) has a unique face-centered cubic lattice structure surrounded by cyanide and iron ferrocyanide [14–16]. PB is also capable of hosting cationic ions with its zeolitic character, thereby enabling the use as a potential adsorbent. Given that the size of PB is well-matched with the size of hydrated cesium ions (3.29 Å), the conceivable significance has made it blossom as an area of research [17]. Nevertheless, this complex regulatory structure requires precise control to be embedded due to its small size of less than 800 nm [18]. In this scenario, tremendous efforts are devoted to target-immobilization on porous adsorbents [19–22].

In this work, we employed activated carbon filters (ACFs) as an anchor for PB. ACFs have been used as a templating material for widely used nanoparticles. While many studies employ N_2 gas for the pore increase during activation, we introduce CO_2 gas before N_2 gas for a better pore-growth as illustrated in Fig. 1. The suggested approach includes the major culprit of global warming as a supporting matrix to insert PB on the adsorbent by the layer-by-layer assembly. ^{137}Cs could possess significant health risks once inhaled

* Corresponding author.
E-mail address: dhsuh@hanyang.ac.kr (D.H. Suh).

https://doi.org/10.1016/j.net.2021.06.006

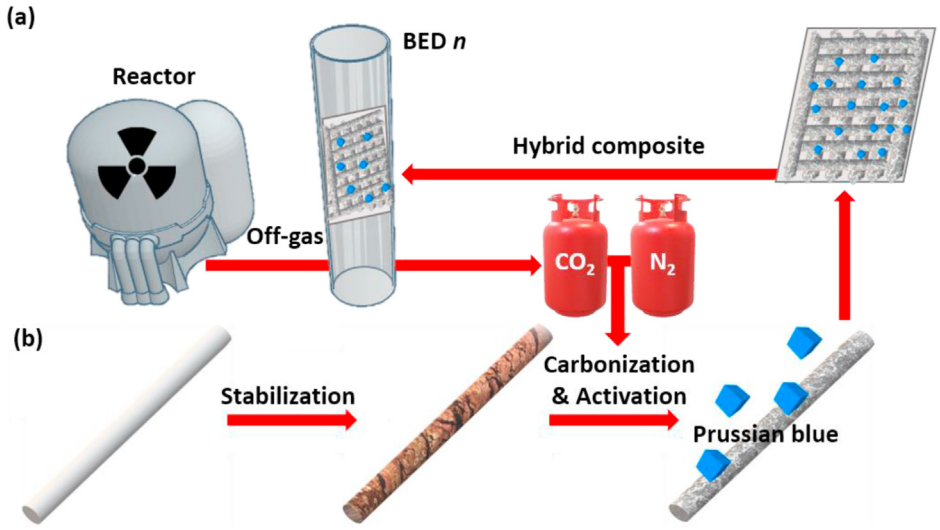

Fig. 1. (a) Schematic representation of a hybrid composite from nuclear reprocessing plants. (b) CO_2 could be collected from the off-gas and further utilized as a green catalyst for the surface modification of ACFs during activation. (For interpretation of the references to color in this figure legend, the reader is referred to the Web version of this article.)

or ingested. Given that ^{133}Cs is a radioisotope of ^{137}Cs, ^{133}Cs was employed for the practical evaluation. We first fabricate CO_2-activated samples and discuss their synergistically enhanced surface properties. The procedures we suggest showed higher loading of PB and ^{133}Cs than vice versa. The adsorption characteristics were further calculated by the energy variations to unveil the physical and chemical mechanisms.

Experimental

All materials and chemicals were of analytical grade and used without further purification. Pyrolysis fuel oil was kindly supported by Hyundai OilBank Corp (Republic of Korea). The facile synthesis of ACF could be realized through stabilization, carbonization, and activation using pyrolysis fuel oil as a starting material [23,24]. First, the temperature was elevated from room temperature to 300 °C under N_2 atmosphere (2 L min^{-1}) for 1 h to remove the impurities. The material was spun in a centrifugal spinneret at temperatures of 250 °C. The resulted samples were then stabilized in the air at 260 °C for another 5 h in the air mood (2 L min^{-1}). The reaction temperature was set as 850 °C for 2 h with a heating rate of 6 °C min^{-1} during carbonization using N_2 gas (2 L min^{-1}). Once the suggested temperature has reached, activation was initiated by adding CO_2 gas (2 L min^{-1}) instead of N_2 gas for 1 h and then cooled to ambient room temperature [25]. Subsequently, 20 mM of powdered PB (Advanced Laboratory of Industrial and Chemical Engineering, Republic of Korea) was stirred with the resulted samples at 120 rpm followed by aging for 3 h to reach a plateau. Based on the synthesis, PB was physically tapped within the pores of ACFs. For comparison, other samples are also prepared without the addition of CO_2 or PB as denoted in Fig. 2. Resulted samples were washed 5 times and dried at 70 °C for 24 h in a desiccator.

To investigate the surface characteristics with the association of CO_2 and/or PB, the specific surface area and following pore volume were measured using Bruanuer-Emmett-Teller and Brunauer-Joyner-Halenda methods (ASAP2460, Micromeritics). The surface morphology was scanned via a scanning electron microscope (S4800, Hitachi). Before loading the samples on the microscope, they were precoated with Au through a sputter coater (E−1045, Hitachi). Elemental characteristics of samples were determined by energy dispersive X-ray spectroscopy (SIGMA, Carl Zeiss). The

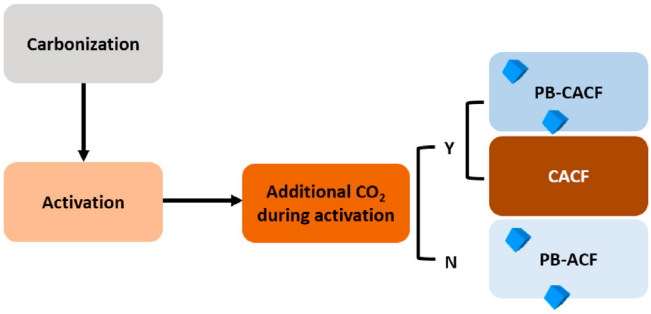

Fig. 2. Sample characterization by differing the synthetic conditions. Such changes are likely to involve inevitable surface decrements or less coordination environment of PB, which might affect the adsorption characteristics and the following energy variations of ^{133}Cs. Within the figure, CACF, PB-ACF, and PB-CACF refer to CO_2-activated carbon filters, activated carbon fibers immobilizing PB, and CO_2-activated carbon filters immobilizing PB, respectively.

binary stability of PB was analyzed by ultraviolet–visible spectrometer (Libra S22, Biochrom). Adsorption characteristics were measured using inductively coupled plasma mass emission spectroscopy at the end of each period (NexION 350D, PerkinElmer). Here, 100 mg of adsorbents and 10 ppm of adsorbate were used, respectively. Thermodynamic parameters were calculated using the thermodynamic equilibrium constant Kd [26,27]. Following that, one could obtain Gibbs free energy change (ΔG^o) using Eq. (1).

$$\Delta G = -RTInKd \quad (1)$$

Accordingly, enthalpy and entropy changes can be calculated by the general thermodynamic expression using Eqs. (2) and (3).

$$\Delta G = \Delta H - T\Delta S \quad (2)$$

$$InKd = (\Delta S/R) - (\Delta H/RT) \quad (3)$$

where R is the universal gas constant (8.314 J mol^{-1} K), T is the absolute temperature (K), ΔH^o is the enthalpy (J mol^{-1} K), and ΔS^o is the entropy (J mol^{-1} K).

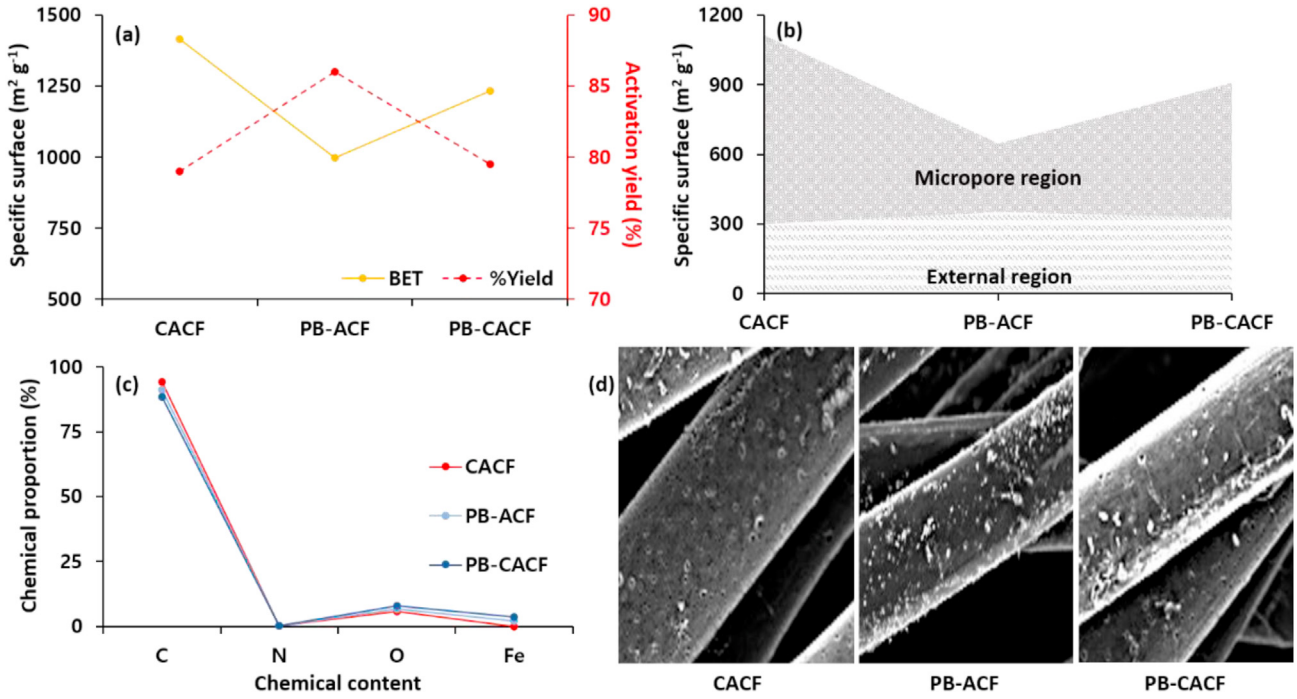

Fig. 3. Surface characteristics of (a) specific surface (left black-colored) and the activation yield of samples (right red-colored) after activation via Brunauer-Emmett-Teller and Brunauer-Joyner-Halenda methods. Proportions of micro- and external regions are plotted in (b). All samples possess a well-developed specific surface of more than 900 $m^2\ g^{-1}$ with a high micropore region over the external region. (c) Chemical contents of samples determined by energy dispersive X-ray spectroscopy. (d) Scanned images with a magnitude of 5.00 K under 2.00 kV. Within the figure, CACF, PB-ACF, and PB-CACF refer to CO_2-activated carbon filters, activated carbon fibers immobilizing PB, and CO_2-activated carbon filters immobilizing PB, respectively. (For interpretation of the references to color in this figure legend, the reader is referred to the Web version of this article.)

Table 1
Brunauer-Emmett-Teller and Brunauer-Joyner-Halenda surface characteristics of samples was determined by N_2 isotherms. Within the table, CACF, PB-ACF, and PB-CACF refer to CO_2-activated carbon filters, activated carbon fibers immobilizing PB, and CO_2-activated carbon filters immobilizing PB, respectively.

Classification	S_{BET}[a] ($m^2\ g^{-1}$)	S_m[b] ($m^2\ g^{-1}$)	S_e[c] ($m^2\ g^{-1}$)	$S_m\ S_{BET}^{-1}$ (%)	$S_e\ S_{BET}^{-1}$ (%)
CACF	1415	1114	301	78.72	21.28
PB-ACF	997	646	351	64.80	35.20
PB-CACF	1233	907	326	73.56	26.44

[a] Brunauer-Emmett-Teller specific surface area.
[b] Micropore region.
[c] External surface region.

Table 2
Elemental characteristics of samples as determined by energy dispersive X-ray spectroscopy. Within the table, CACF, PB-ACF, and PB-CACF refer to CO_2-activated carbon filters, activated carbon fibers immobilizing PB, and CO_2-activated carbon filters immobilizing PB, respectively.

Classification	Chemical proportion (%)			
	C	N	O[a]	Fe
CACF	94.12	0.24	5.64	–
PB-ACF	91.10	0.25	6.51	2.14
PB-CACF	88.32	0.24	7.92	3.52

[a] O content was obtained by mass difference.

2. Results and discussion

Additional CO_2 gas during activation allows for the pore growth of samples. Surface characteristics and the activation yield were in a non-linear correlation due to the pore growth (Fig. 3(a)-3(b) and Table 1). Both the specific surface and micropore region were in the order of C-ACF > PB-CACF > PB-ACF. This suggests that micropores

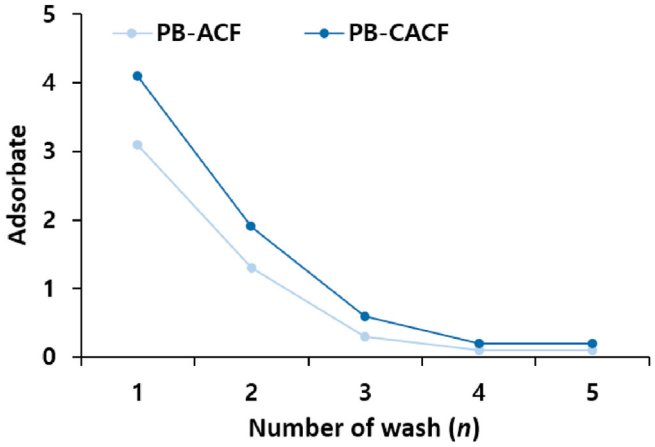

Fig. 4. Leaching of PB probed by ultraviolet–visible spectrometer for 5 times of wash. Within the figure, PB-ACF and PB-CACF refer to activated carbon fibers immobilizing PB, and CO_2-activated carbon filters immobilizing PB, respectively.

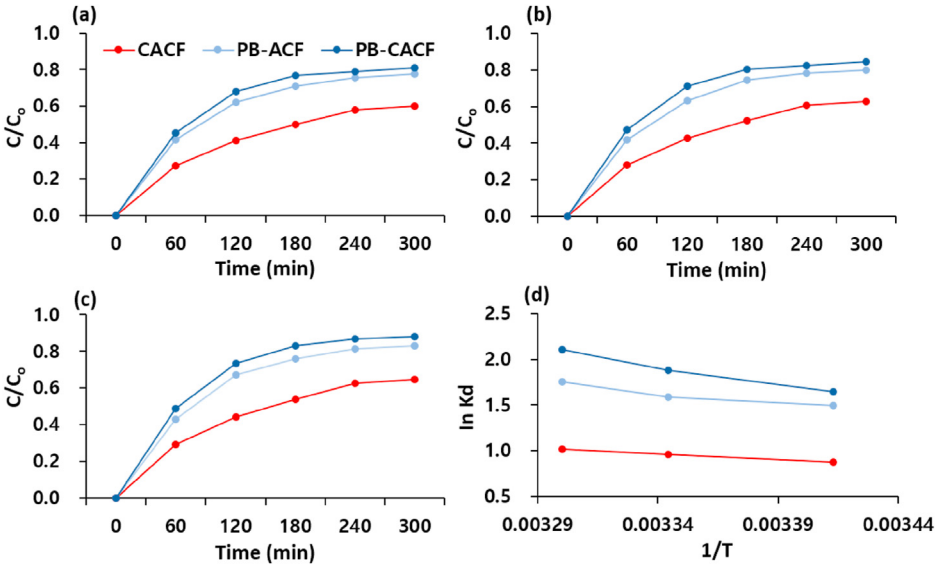

Fig. 5. Plots of ^{133}Cs adsorption onto samples at designated temperature ranges of (a) 25 °C, (b) 30 °C, and (c) 35 °C. Adsorption characteristics were measured using inductively coupled plasma mass emission spectroscopy at the end of each period. The values were averaged after 10 trials. Thermodynamic parameters are plotted in (d) with the regression coefficient > 0.9. All figures follow the same legend as listed in (a). Within the figure, CACF, PB-ACF, and PB-CACF refer to CO_2-activated carbon filters, activated carbon fibers immobilizing PB, and CO_2-activated carbon filters immobilizing PB, respectively.

Table 3
Adsorption performance (C/C_o) of ^{133}Cs onto samples at designated temperature ranges of 25 °C, 30 °C, and 35 °C. Within the table, CACF, PB-ACF, and PB-CACF refer to CO_2-activated carbon filters, activated carbon fibers immobilizing PB, and CO_2-activated carbon filters immobilizing PB, respectively.

Classification	Temperature (°C)	Error (n = 10)	Time (min)				
			60	**120**	**180**	**240**	**300**
CACF	20	Avg.	0.27	0.41	0.50	0.58	0.60
		Min.	0.24	0.39	0.49	0.58	0.59
		Max.	0.30	0.43	0.51	0.58	0.61
	25	Avg.	0.28	0.43	0.52	0.61	0.63
		Min.	0.25	0.38	0.48	0.59	0.63
		Max.	0.31	0.48	0.56	0.63	0.63
	30	Avg.	0.30	0.45	0.56	0.64	0.65
		Min.	0.27	0.42	0.54	0.63	0.64
		Max.	0.33	0.48	0.58	0.65	0.66
PB-ACF	20	Avg.	0.43	0.63	0.72	0.76	0.79
		Min.	0.40	0.61	0.71	0.75	0.79
		Max.	0.46	0.65	0.73	0.77	0.79
	25	Avg.	0.43	0.64	0.75	0.79	0.81
		Min.	0.39	0.61	0.73	0.77	0.80
		Max.	0.47	0.67	0.77	0.81	0.82
	30	Avg.	0.44	0.68	0.77	0.82	0.83
		Min.	0.39	0.63	0.74	0.80	0.84
		Max.	0.49	0.73	0.80	0.84	0.85
PB-C-ACF	20	Avg.	0.45	0.69	0.78	0.80	0.82
		Min.	0.42	0.66	0.77	0.79	0.82
		Max.	0.48	0.72	0.79	0.81	0.82
	25	Avg.	0.48	0.72	0.81	0.83	0.85
		Min.	0.45	0.70	0.80	0.82	0.85
		Max.	0.51	0.74	0.82	0.84	0.85
	30	Avg.	0.50	0.74	0.84	0.88	0.89
		Min.	0.44	0.72	0.83	0.87	0.88
		Max.	0.56	0.76	0.85	0.89	0.90

may preserve the size of PB in the colloid. In typical pitch-based ACFs, the loading amount of N is usually due to the starting material. Fe was observed in cases of PB treatment (Fig. 3(c) and Table 2). As for the CACF, only the basic chemical elements of C, N, and O were indicated. Considering the effect of the loading amount of PB, we further tracked the surface with scanned images (Fig. 3(d)). PB was more likely to be observed on the surface in the case of PB-ACF, whereas less snowflake-looking PB can be seen in PB-CACF. PB-CACF also showed 24.39% better leaching of PB than PB-ACF during the first trial of washing (Fig. 4). In all cases, leaching of PB declines after the first trial mainly due to the weak bonding between PB and micropores. We note that the use of PB should be thoroughly examined by optimizing the design of pores from the environmental perspective of reusability. We conclude that the aid of CO_2 increases the micropore region over the external region in a sufficient manner, thus allowing more spots for PB to be adsorbed.

Table 4
Thermodynamic parameters of ^{133}Cs adsorption onto samples at various temperature ranges. Within the table, CACF, PB-ACF, and PB-CACF refer to CO_2-activated carbon filters, activated carbon fibers immobilizing PB, and CO_2-activated carbon filters immobilizing PB, respectively.

Classification	Temperature (°C)	ΔG^o (kJ mol^{-1} K)	ΔH^o (kJ mol^{-1} K)	ΔS^o (kJ mol^{-1} K)
CACF	25	−2.1326	10.2054	42.1021
	30	−2.3779		
	35	−2.5549		
PB-ACF	25	−3.6342	18.7522	76.2718
	30	−3.9507		
	35	−4.4206		
PB-C-ACF	25	−3.9988	33.9901	129.565
	30	−4.6785		
	35	−5.3108		

The Results of ^{133}Cs adsorption indicate that the increase in the temperature slightly increased the amount of adsorbate to samples (Fig. 5(a)-5(c) and Table 3). To put it in other words, the amount of PB is the primary factor for ^{133}Cs adsorption. A possible explanation may be that CACF with the most significant surface characteristics did not show good adsorption performance among other PB-loaded samples. PB-CACF, a sample with relatively high surface characteristics and the highest PB-loaded sample, showed 26.14% and 5.68% more ^{133}Cs adsorption capacity at 35 °C compared to CACF and PB-ACF, respectively. Interestingly, PB-ACF also revealed 21.69% more ^{133}Cs adsorption capacity compared to CACF. With these features in hands, ^{133}Cs adsorption is regulated by the surrounding environment in the order of the amount of PB > surface characteristics > temperature. Thermodynamic parameters are listed in Fig. 5(d) and Table 4. ΔH^o and ΔS^o were determined by the values from the slope and intercept. The change of ΔG^o in the range of nil to −20 kJ mol^{-1} suggests the physical adsorption, and that for the chemical adsorption is in the range of −80 to −400 kJ mol^{-1} [28]. The overall trend of ΔG^o during the adsorption was in the range of −5.3108 to −2.1326 kJ mol^{-1} for the calculated range of temperatures. The results demonstrated that the observed adsorption is a spontaneous and feasible physical process [29,30]. Negative ΔG^o values also confirmed that the adsorption process becomes more favorable at higher temperatures (ΔG^o < 0, exergonic). A ΔH^o less than 42 kJ mol^{-1} also indicated the dominance of the physical adsorption over the chemical adsorption process. The positive trend of ΔS^o shows the affinity of ^{133}Cs and the increasing randomness at the solid-solution interface during the adsorption process. The overall thermodynamic parameters are in good agreement with the relevant studies using PB for cesium adsorption [31,32].

3. Concluding remarks

The foregoing Results demonstrate a rare example of CO_2-ACFs for the immobilization of PB. We revealed that the adsorption of ^{133}Cs was more effective in the order of the loading of PB > surface characteristics > temperature. As a result, PB-CACF showed the highest adsorption capacity of ^{133}Cs compared to other counterparts. More importantly, we also demonstrated the adsorption characteristics with the aid of energy variations. The change of ΔG^o in the range of nil to −20 kJ mol^{-1} with increased temperature showed the trend of physical adsorption. Positive values of ΔH^o revealed feasible and endothermic adsorption processes. Increased randomness at the solid-solution interface during adsorption was also confirmed by positive values of ΔS^o. In all cases, the holding of PB from ACFs cannot be easily managed after the first trial. There are some potential approaches that could overcome this issue, including in-situ physiochemical PB synthesis inside the rich pores of ACFs. In summarization, this work not only reports the unique immobilization method, but also provides the adsorption characteristics via energy variations for the advanced remediation of critical radionuclides.

Declaration of competing interest

The authors declare that they have no known competing financial interests or personal relationships that could have appeared to influence the work reported in this paper.

References

[1] E. Park, Positive or negative? Public perceptions of nuclear energy in South Korea: evidence from big data, Nucl. Eng. Techonol. 51 (2) (2019) 626–630, https://doi.org/10.1016/j.net.2018.10.025.
[2] L. Geng, T. Liu, K. Zhou, G. Yang, Can power affect environmental risk attitude toward nuclear energy? Energy Pol. 113 (2018) 87–93, https://doi.org/10.1016/j.enpol.2017.10.051.
[3] E.O. Adamov, V.I. Rachkov, New technological platform for the national nuclear energy strategy development, Therm. Eng. 64 (2017) 945–951, https://doi.org/10.1134/S004060151713002X.
[4] N. Mahmood, Z. Wang, B. Zhang, The role of nuclear energy in the correction of environmental pollution: evidence from Pakistan, Nucl. Eng. Techonol. 52 (6) (2020) 1327–1333, https://doi.org/10.1016/j.net.2019.11.027.
[5] J.H. Song, T. Kim, J.W. Yeon, Radioactivity data analysis of 137Cs in marine sediments near severely damaged Chernobyl and Fukushima nuclear power plants, Nucl. Eng. Techonol. 52 (2) (2020) 366–372, https://doi.org/10.1016/j.net.2019.07.017.
[6] T. Sasaki, D. Matoba, T. Dohi, K. Fujiwara, T. Kobayashi, K. Iijima, Vertical distribution of 90Sr and 137Cs in soils near the Fukushima Daiichi nuclear power station, J. Radioanal. Nucl. Chem. 326 (2020) 303–314, https://doi.org/10.1007/s10967-020-07294-3.
[7] A. Bilici, S. Bilici, F. Külahcı, Statistical analysis for 134Cs and 137Cs radioactivity risk levels modeling, J. Radioanal. Nucl. Chem. 326 (2020) 1047–1064, https://doi.org/10.1007/s10967-020-07399-9.
[8] E.A. Abdel-Galil, R.S. Hassan, M.A. Eid, Assessment of nano-sized stannic silicomolybdate for the removal of 137Cs, 90Sr, and 141Ce radionuclides from radioactive waste solutions, Appl. Radiat. Isot. 148 (2019) 91–101, https://doi.org/10.1016/j.apradiso.2019.03.029.
[9] S.S. Choi, J.H. Lee, Y.M. Jin, S.H. Lee, Adsorption characteristics of volatile organic compounds onto lyocell-based activated carbon fibers, Carbon. Lett. 29 (2019) 633–642, https://doi.org/10.1007/s42823-019-00063-7.
[10] K.C. Khulbe, T. Matsuura, Removal of heavy metals and pollutants by membrane adsorption techniques, Appl. Water. Sci. 8 (2018) 19, https://doi.org/10.1007/s13201-018-0661-6.
[11] X. Liu, R. Tian, W. Ding, H. Yunhua, L. Hang, Adsorption selectivity of heavy metals by Na-clinoptilolite in aqueous solutions, Adsorption 25 (2019) 747–755, https://doi.org/10.1007/s10450-019-00081-x.
[12] M.N. Sahmoune, Evaluation of thermodynamic parameters for adsorption of heavy metals by green adsorbents, Environ. Chem. Lett. 17 (2019) 697–704, https://doi.org/10.1007/s10311-018-00819-z.
[13] A.G. Varghese, S.A. Paul, M.S. Latha, Remediation of heavy metals and dyes from wastewater using cellulose-based adsorbents, Environ. Chem. Lett. 17 (2019) 867–877, https://doi.org/10.1007/s10311-018-00843-z.
[14] A. Shahzad, M. Moztahida, K. Tahir, B. Kim, H. Jeon, A.A. Ghani, D.S. Lee, Highly effective prussian blue-coated MXene aerogel spheres for selective removal of cesium ions, J. Nucl. Mater. 539 (2020) 152277, https://doi.org/10.1016/j.jnucmat.2020.152277.
[15] J. Wang, S. Zhuang, Y. Liu, Metal hexacyanoferrates-based adsorbents for cesium removal, Coord. Chem. Rev. 374 (2018) 430–438, https://doi.org/10.1016/j.ccr.2018.07.014.
[16] M.M.S. Ali, N.M. Sami, A.A. El-Sayed, Removal of Cs+, Sr2+ and Co2+ by activated charcoal modified with Prussian blue nanoparticle (PBNP) from aqueous media: kinetics and equilibrium studies, J. Radioanal. Nucl. Chem.

324 (2020) 189–201, https://doi.org/10.1007/s10967-020-07067-y.
[17] H. Kim, H. Wi, S. Kang, S. Yoon, S. Bae, Y. Hwang, Prussian blue immobilized cellulosic filter for the removal of aqueous cesium, Sci. Total Environ. 670 (2019) 779–788, https://doi.org/10.1016/j.scitotenv.2019.03.234.
[18] M.A. Komkova, A.A. Zarochintsev, E.E. Karyakina, A.A. Karyakin, Electrochemical and sensing properties of Prussian Blue based nanozymes "artificial peroxidase", J. Electroanal. Chem. 872 (2020) 114048, https://doi.org/10.1016/j.jelechem.2020.114048.
[19] P. Rauwel, E. Rauwel, Towards the extraction of radioactive cesium-137 from water via graphene/CNT and nanostructured prussian blue hybrid nanocomposites: a review, Nanomaterials 9 (5) (2019) 682, https://doi.org/10.3390/nano9050682.
[20] A.M. Alansi, M. Al-Qunaibit, I.O. Alade, T.F. Qahtan, T.A. Saleh, Visible-light responsive BiOBr nanoparticles loaded on reduced graphene oxide for photocatalytic degradation of dye, J. Mol. Liq. 253 (2018) 297–304, https://doi.org/10.1016/j.molliq.2018.01.034.
[21] A.M. Alansi, T.F. Qahtan, T.A. Saleh, Solar-driven fixation of bismuth oxyhalides on reduced graphene oxide for efficient sunlight-responsive immobilized photocatalytic systems, Adv. Mater. Interfaces 8 (3) (2021) 2001463, https://doi.org/10.1002/admi.202001463.
[22] T.A. Saleh, Nanomaterials: classification, properties, and environmental toxicities, Environ. Technol. Innov. (2020) 101067, https://doi.org/10.1016/j.eti.2020.101067.
[23] W. Chen, F. He, S. Zhang, H. Xv, Z. Xv, Development of porosity and surface chemistry of textile waste jute-based activated carbon by physical activation, Environ. Sci. Pollut. Res. 25 (2018) 9840–9848, https://doi.org/10.1007/s11356-018-1335-.
[24] J.H. Lee, S.H. Lee, D.H. Suh, High micropore number and specific surface of carbon fibers pretreated with a swarm of CO2 micro–nanobubbles, Environ. Chem. Lett. (2021) 1–7, https://doi.org/10.1007/s10311-021-01243-6.
[25] S.N. Farhan, A.A. Khadom, Biosorption of heavy metals from aqueous solutions by Saccharomyces Cerevisiae, Int. J. Ind. Chem. 6 (2015) 119–130, https://doi.org/10.1007/s40090-015-0038-8.
[26] M. Tuzen, A. Sarı, T.A. Saleh, Synthesis, characterization and evaluation of carbon nanofiber modified-polymer for ultra-removal of thorium ions from aquatic media, Chem. Eng. Res. Des. 163 (2020) 76–84, https://doi.org/10.1016/j.cherd.2020.08.021.
[27] M. Tuzen, T.A. Saleh, A. Sarı, Interfacial polymerization of trimesoyl chloride with melamine and palygorskite for efficient uranium ions ultra-removal, Chem. Eng. Res. Des. 159 (2020) 353–361, https://doi.org/10.1016/j.cherd.2020.04.034.
[28] M. Hadadian, E.K. Goharshadi, M.M. Fard, H. Ahmadzadeh, Synergistic effect of graphene nanosheets and zinc oxide nanoparticles for effective adsorption of Ni (II) ions from aqueous solutions, Appl. Phys. A 124 (2018) 239, https://doi.org/10.1007/s00339-018-1664-8.
[29] G. Özsin, M. Kılıç, E. Apaydın-Varol, A. Eren Putun, Chemically activated carbon production from agricultural waste of chickpea and its application for heavy metal adsorption: equilibrium, kinetic, and thermodynamic studies, Appl. Water. Sci. 9 (2019) 56, https://doi.org/10.1007/s13201-019-0942-8.
[30] J.H. Lee, S.H. Lee, D.H. Suh, Using nanobubblized carbon dioxide for effective microextraction of heavy metals, J. CO2. Util. 39 (2020) 101163, https://doi.org/10.1016/j.jcou.2020.101163.
[31] J. Li, Y. Zan, Z. Zhang, M. Dou, F. Wang, Prussian blue nanocubes decorated on nitrogen-doped hierarchically porous carbon network for efficient sorption of radioactive cesium, J. Hazard Mater. 385 (2020) 121568, https://doi.org/10.1016/j.jhazmat.2019.121568.
[32] A.M.S. El-Din, T. Monir, M.A. Sayed, Nano-sized Prussian blue immobilized costless agro-industrial waste for the removal of cesium-137 ions, Environ. Sci. Pollut. Res. 26 (2019) 25550–25563, https://doi.org/10.1007/s11356-019-05851-2.